

# On marginals and profiled posteriors for cosmological parameter estimation

Martin Kerscher<sup>a</sup> Jochen Weller<sup>a,b</sup>

<sup>a</sup>Ludwig-Maximilians Universität München, Universitäts-Sternwarte München, Fakultät für Physik, Scheinerstr. 1, 81679 München, Germany

<sup>b</sup>Max Planck Institute for Extraterrestrial Physics, Giessenbachstr. 1, 85748 Garching, Germany

E-mail: [martin.kerscher@lmu.de](mailto:martin.kerscher@lmu.de)

**Abstract.** With several examples and in an analysis of the Pantheon+ supernova sample we discuss the properties of the marginal posterior distribution versus the profiled posterior distribution – the profile likelihood in a Bayesian disguise. We investigate whether maximisation, as used for the profiling, or integration, as used for the marginalisation, is more appropriate. To report results we recommend the marginal posterior distribution.

**Keywords:** Bayesian reasoning, Frequentist statistics, supernova type Ia - standard candles

---

## Contents

<b>1</b>	<b>Introduction</b>	<b>1</b>
<b>2</b>	<b>Marginalisation and profiling</b>	<b>2</b>
2.1	Profile likelihood	3
2.2	Profiled posterior	3
2.3	Laplace approximation	4
2.4	The profiled posterior as the marginal of a Bayesian hierarchical model	5
<b>3</b>	<b>Example Distributions</b>	<b>5</b>
3.1	A Gaussian Distribution	6
3.2	A model for the volume effect	7
3.3	A model with a ridge	9
3.4	A Rosenbrock function	10
3.4.1	A Rosenbrock distribution with added noise	12
<b>4</b>	<b>Cosmological parameters from the SN Ia magnitude redshift relation</b>	<b>13</b>
4.1	The sample, the models and the analysis	13
4.2	Marginal and profiled posterior distribution of the parameters	15
4.2.1	Flat $w$ CDM and non-flat $\Lambda$ CDM	15
4.2.2	Non-flat $w$ CDM	16
4.3	Summary of the one-dimensional distributions	18
<b>5</b>	<b>Conclusions</b>	<b>19</b>

---

## 1 Introduction

Cosmological models use several parameters like the matter content, a dark energy component, or the Hubble parameter etc. In a Bayesian analysis, the posterior distribution of these parameters is determined from astronomical observations (e.g. [1]). In addition, further nuisance parameters may enter the analysis. To focus on a subset of the cosmological parameters, the marginal of the posterior distribution is used to report the one-dimensional distribution itself, the mean parameter values, or credible regions. As an alternative, the profile likelihood has been used [2–5]. To focus on one parameter, one sets the other parameters to the values maximising the likelihood. The function of the remaining parameter is called the profile likelihood. Together with standard methods from classical statistics, this profile likelihood can be used to determine the confidence region for a parameter (see e.g. [6]). Profiling and marginalisation may give concordant and sometimes differing results for the parameters. For the cosmic radiation density this has been investigated by [7], for an early dark energy model see [8], for an entangled initial quantum state see [9], and for the tensor-to-scalar ratio see [10].

It is common to attribute the differences between marginalisation and profiling to a volume effect: If the maximum of the posterior is not surrounded by a region with a large fraction of the posterior mass, the marginalisation and profiling will give different results. An example with a sum of two Gaussians illustrating the volume effect was given by [11].

She develops methods for a fast detection of a volume effect. Hadzhiyska et al. [12] use the Laplace approximation centred on values of the profiled posterior to factorise the full marginal posterior into the profiling part and their Laplace term. Recently Raveria et al. [13] use this factorisation of [12] and are able to distinguish the volume effect from the so called projection effect. In some of our examples and for the supernova data analysis using the flat  $w$ CDM and non-flat  $\Lambda$ CDM this Laplace approximation is indistinguishable from the marginal posterior. However in addition we study the limitations of this approximation in more complex correlated settings. Specifically for non-convex credibility regions the profiled posterior and consequently the Laplace approximation may ignore a branch from the full posterior. The maximum from the profiling may jump between the branches, leading to discontinuities in the Laplace approximation and to significant differences between the profiled and the marginalised posterior.

In section 2 we briefly review the basics of parameter estimation. We construct a special posterior distribution following a similar procedure as used for profiling the likelihood, and call this the profiled posterior distribution – the profile likelihood in a Bayesian disguise (see also [7, 12, 14]). Following Hadzhiyska et al. [12] we give the Laplace approximation to the marginalised posterior. Then we show that the profiled posterior is a marginal distribution of a special Bayesian hierarchical model. Both the profiled posterior and the marginal posterior distribution are probability densities for the parameters under consideration. Therefore, we can compare them directly. Taking the perspective from classical statistics, that is hardly a fair procedure, since we are missing the point, that in the classical approach there is no distribution of the parameters. This difference between the classical and the Bayesian approach cannot be reconciled. Here we stick to the Bayesian description, because this reformulation allows us to compare the distributions obtained from maximisation or from integration on an equal footing. In section 3, we discuss the properties of the distributions for several examples. For a simple Gaussian model, the marginal and profiled posterior agree. But we also consider a model with a tuneable volume effect and a model with non-convex credible regions where distinct differences show up. In section 4 we compare the profiled and the marginal posterior distributions of cosmological parameters, obtained from an analysis of the supernova magnitude redshift relation using the Pantheon+ supernova sample [15]. We use this to highlight the differences between profiling and marginalisation. In the CMB case as discussed in [7–10] the differences between profiling and marginalisation are either small or may be attributed to a volume effect. The shown credibility regions are mainly convex. In our analysis of the supernova sample we observe a pathology going beyond the simple volume effect. There non-convex credibility regions show up and the profiling and marginalisation lead to quantitatively and qualitatively different results. In section 5 we present arguments why we think that the marginal posterior distributions should be the preferred way to report results from a parameter estimation.

## 2 Marginalisation and profiling

We start with a classic setting for parameter estimation. Consider a model with parameters  $(\theta_1, \dots, \theta_d) = \Theta \in \mathbb{R}^d$ . We constrain these parameters with the observed data  $\mathbf{d}$ . Bayes theorem gives us the posterior distribution of the parameters

$$p(\Theta|\mathbf{d}) = \frac{\mathcal{L}(\mathbf{d}|\Theta) p(\Theta)}{p(\mathbf{d})}. \quad (2.1)$$

The prior distribution  $p(\Theta)$  is quantifying our prior knowledge about the parameters, the likelihood  $\mathcal{L}(\mathbf{d}|\Theta)$  is the probability of the data given a set of parameters, and  $p(\mathbf{d})$  is the normalisation, also called the evidence. We are also interested in the distribution of only the  $i$ th parameter  $\theta_i$ . The rest of the parameters is indicated by  $\Theta_{\setminus i} = (\theta_1, \dots, \theta_{i-1}, \theta_{i+1}, \dots, \theta_d) \in \mathbb{R}^{d-1}$ . Here we focus on *one* parameter  $\theta_i$ , but analogously a subset of parameters could be considered. In the following, we will also write  $\theta_i, \Theta_{\setminus i}$  together and identify this with the full set of the parameters  $\Theta \in \mathbb{R}^d$ . The marginal posterior distribution is given by

$$p(\theta_i|\mathbf{d}) = \int p(\theta_i, \Theta_{\setminus i}|\mathbf{d}) \, d\Theta_{\setminus i}. \quad (2.2)$$

In a Bayesian analysis, this marginal posterior can be used to derive a credible region for  $\theta_i$  or calculate its maximum or mean value. The maximum likelihood estimate  $\tilde{\Theta}$  is defined by

$$\tilde{\Theta} = \arg \max_{\Theta} \mathcal{L}(\mathbf{d}|\Theta). \quad (2.3)$$

For an unimodal likelihood function,  $\mathcal{L}(\mathbf{d}|\Theta)$  the  $\tilde{\Theta}$  is unique. From the likelihood, we can also determine the confidence regions using e.g. a likelihood ratio test [6, 16].

## 2.1 Profile likelihood

The profile likelihood of the parameter  $\theta_i$  is defined as the function

$$\mathcal{L}_p(\theta_i) = \max_{\Theta_{\setminus i}} \mathcal{L}(\mathbf{d}|\theta_i, \Theta_{\setminus i}). \quad (2.4)$$

For each value of  $\theta_i$  we determine the maximum of the likelihood over the remaining parameters  $\Theta_{\setminus i}$ . Correspondingly, the mapping

$$\mathbf{t}_{\setminus i}(\theta_i) = \arg \max_{\Theta_{\setminus i}} \mathcal{L}(\mathbf{d}|\theta_i, \Theta_{\setminus i}) \quad (2.5)$$

assigns to each parameter value  $\theta_i \in \mathbb{R}$  the parameters  $\hat{\Theta}_{\setminus i} \in \mathbb{R}^{d-1}$ , where the likelihood is at its maximum. If the maximum is unique, the  $(\theta_i, \mathbf{t}_{\setminus i}(\theta_i)) \in \mathbb{R}^d$  defines the graph of  $\mathbf{t}_{\setminus i}$  in the full parameter space. We call it the profiling graph. Now the profile likelihood can be written as

$$\mathcal{L}_p(\theta_i) = \mathcal{L}(\mathbf{d}|\theta_i, \mathbf{t}_{\setminus i}(\theta_i)). \quad (2.6)$$

The conditioning on this graph does not necessarily lead to a new likelihood. But at least asymptotically, near the maximum, the profile likelihood behaves like a likelihood and allows the construction of approximate confidence sets [17]. The profile likelihood  $\mathcal{L}_p(\theta_i)$  may be used to determine the confidence interval around the maximum likelihood estimate of the single parameter  $\tilde{\theta}_i$ . No integration is used, but with the maximisation procedure we follow the graph  $(\theta_i, \mathbf{t}_{\setminus i}(\theta_i))$  in parameter space.

## 2.2 Profiled posterior

To construct a Bayesian analogue of the profile likelihood, we use a similar procedure as in Eqn. (2.4), but now we are profiling the posterior distribution  $p(\Theta|\mathbf{d})$ . The function

$$r(\theta_i) = \max_{\Theta_{\setminus i}} p(\theta_i, \Theta_{\setminus i}|\mathbf{d}). \quad (2.7)$$

is not a probability density, but since  $r(\theta_i) \geq 0$  we may calculate the normalisation  $c_i = \int r(\theta_i) d\theta_i$  and define a probability density for  $\theta_i$  by,

$$p_p(\theta_i|\mathbf{d}) = \frac{1}{c_i} \max_{\Theta_{]i[}} p(\theta_i, \Theta_{]i[}|\mathbf{d}). \quad (2.8)$$

We call this  $p_p(\theta_i|\mathbf{d})$  the profiled posterior (see also [7, 12, 14]). For a flat prior  $p(\Theta) = a$  and with Eqns. (2.1) and (2.6) we get,

$$p_p(\theta_i|\mathbf{d}) = \frac{a}{c_i p(\mathbf{d})} \max_{\Theta_{]i[}} \mathcal{L}(\mathbf{d}|\theta_i, \Theta_{]i[}) = \frac{a}{c_i p(\mathbf{d})} \mathcal{L}(\mathbf{d}|\theta_i, \mathbf{t}_{]i[}(\theta_i)) \propto \mathcal{L}_p(\theta_i). \quad (2.9)$$

Hence the profiled posterior  $p_p$  is the Bayesian analogue of the profile likelihood  $\mathcal{L}_p$ . Throughout this article, we will use flat priors because we want to emphasise the connection between the profiled posterior distribution and the profile likelihood. A flat prior  $p(\Theta) = a$  on the full parameter space  $\mathbb{R}^d$  is not normalisable, but we can work around this. The argument above, showing the proportionality of the profile likelihood and the profiled posterior (2.9), is still valid if  $\mathcal{L}(\mathbf{d}|\cdot)$  has a finite support  $A \subset \mathbb{R}^d$  and we choose the uniform prior  $p(\Theta) = a$  for  $\Theta \in A$  and zero otherwise. Then  $1/a = \text{vol}(A)$  is the  $d$ -dimensional volume of  $A$ . This restriction of the prior to a set  $A$  can also be done approximately as long as  $\mathcal{L}(\mathbf{d}|\Theta) \ll 1$  for  $\Theta \notin A$ . The profiled posterior  $p_p(\theta_i|\mathbf{d})$  and the marginal posterior  $p(\theta_i|\mathbf{d})$  are both probability densities for the parameter  $\theta_i$ . This is the basis for the comparison done in section 3 and 4.

### 2.3 Laplace approximation

In the vicinity of its maximum the posterior can be approximated by a Gaussian which is called the Laplace approximation [18, 19]. Hadzhiyska et al. [12] used a similar approximation to determine the posterior distribution by

$$p(\theta_i, \Theta_{]i[}|\mathbf{d}) \approx p_p(\theta_i|\mathbf{d}) \exp\left(-\frac{1}{2}\Delta^T \mathcal{F}(\theta_i)\Delta\right), \quad (2.10)$$

where  $\Delta = (\Theta_{]i[} - \mathbf{t}_{]i[}(\theta_i))^T$  and

$$\mathcal{F}_{lm}(\theta_i) = \frac{1}{2} \frac{\partial^2}{\partial\phi_l \partial\phi_m} \log p(\theta_i, \Phi|\mathbf{d})|_{\Phi=\mathbf{t}_{]i[}(\theta_i)} \quad (2.11)$$

with  $\Phi = (\phi_1, \dots, \phi_{d-1})$  for  $l, m = 1, \dots, d-1$ . This is a Laplace approximation of the posterior with fixed  $\theta_i$  around the value  $\mathbf{t}_{]i[}(\theta_i)$ , as given by the profiling procedure. Hence the Gaussian integral over  $\Theta_{]i[}$  in Eqn. (2.2) can be performed, and is resulting in the Laplace approximation  $p_L(\theta_i|\mathbf{d})$  of the marginal  $p(\theta_i|\mathbf{d})$  as

$$p_L(\theta_i|\mathbf{d}) = C \frac{p_p(\theta_i|\mathbf{d})}{\sqrt{\det \mathcal{F}(\theta_i)}}. \quad (2.12)$$

All terms independent of  $\theta_i$  are merged into the normalisation factor  $C$ . As illustrated by Hadzhiyska et al. [12] this leads to a significant speed-up in calculations of the marginal posterior. Even for complex posteriors this Laplace approximation can be a good choice, as long as for each  $\theta_i$  the posterior is close to a Gaussian in the remaining parameters  $\Theta_{]i[}$ . We will show this in the following examples and in the analysis of the supernova sample, but we will also see that in certain situations the approximate  $p_L(\theta_i|\mathbf{d})$  differs from  $p(\theta_i|\mathbf{d})$  significantly.

## 2.4 The profiled posterior as the marginal of a Bayesian hierarchical model

Before we turn to the examples, we will show that the profiled posterior, and consequently the profile likelihood, can be understood as a marginal distribution of a special Bayesian hierarchical model. In a hierarchical model, we use a further hyper-parameter  $\phi$  to model the dependencies between the parameters  $\Theta = (\theta_1, \dots, \theta_d)$ . The extended model with the hyper-parameter  $\phi$  leads to the following Bayesian update for the posterior distribution of  $\Theta$  and  $\phi$

$$p(\Theta, \phi | \mathbf{d}) = \frac{\mathcal{L}(\mathbf{d} | \Theta, \phi) p(\Theta, \phi)}{p(\mathbf{d})} = \frac{\mathcal{L}(\mathbf{d} | \Theta, \phi) p(\Theta | \phi) p_h(\phi)}{p(\mathbf{d})}. \quad (2.13)$$

The prior distribution  $p(\Theta, \phi)$  factorises into the conditional prior distribution  $p(\Theta | \phi)$  of  $\Theta$  depending on  $\phi$ , and the hyper-prior  $p_h(\phi)$ . Often the likelihood  $\mathcal{L}(\mathbf{d} | \Theta, \phi) = \mathcal{L}(\mathbf{d} | \Theta)$  is not directly depending on the hyper-parameter  $\phi$ . Also, further levels are possible, but for our application a simple one-level hierarchy is enough. The profiling procedure defines the mapping  $\mathbf{t}_{j|i}(\theta_i) = \hat{\Theta}_{j|i}$  (see Eqn. (2.5)) and allows us to determine the parameters  $\hat{\Theta}_{j|i}$  depending on the value of the parameter  $\theta_i$ . We model this strict dependency in the conditional distribution  $p(\Theta | \phi)$  using Dirac  $\delta$  distributions

$$p(\Theta | \phi) = \delta(\phi - \theta_i) \delta(\mathbf{t}_{j|i}(\theta_i) - \Theta_{j|i}), \quad (2.14)$$

with  $\Theta = (\theta_i, \Theta_{j|i})$ . Given  $\phi$ , this definition specifies a probability distribution for  $\Theta$ , since  $p(\Theta | \phi) \geq 0$  for any  $\Theta$ , and also  $\int p(\Theta | \phi) d\Theta = 1$ . As before, we are interested in the distribution of  $\theta_i$ , hence we integrate over  $\Theta_{j|i}$  and also the hyper-parameter  $\phi$  to obtain the marginal posterior  $p_h(\theta_i | \mathbf{d})$  for this hierarchical model.

$$\begin{aligned} p_h(\theta_i | \mathbf{d}) &= \int_{\mathbb{R}^{d-1}} \int_{\mathbb{R}} p(\theta_i, \Theta_{j|i}, \phi | \mathbf{d}) d\phi d\Theta_{j|i} \\ &= \int_{\mathbb{R}^{d-1}} \int_{\mathbb{R}} \frac{1}{p(\mathbf{d})} \mathcal{L}(\mathbf{d} | \theta_i, \Theta_{j|i}) \delta(\phi - \theta_i) \delta(\mathbf{t}_{j|i}(\theta_i) - \Theta_{j|i}) p_h(\phi) d\phi d\Theta_{j|i} \\ &= \frac{1}{p(\mathbf{d})} \mathcal{L}(\mathbf{d} | \theta_i, \mathbf{t}_{j|i}(\theta_i)) p(\theta_i) = \frac{p(\theta_i)}{p(\mathbf{d})} \mathcal{L}_p(\theta_i). \end{aligned} \quad (2.15)$$

Here we assume that the likelihood has no explicit dependence on the hyper-parameter  $\phi$  and that the prior distribution for the parameter  $\theta_i$  is equal to the hyper-prior  $p_h(\theta_i) = p(\theta_i)$ . If we assume a flat prior for the parameters, we see that the marginal of this hierarchical model is equal to the profiled posterior of Eqn. (2.9):

$$p_h(\theta_i | \mathbf{d}) = p_p(\theta_i | \mathbf{d}). \quad (2.16)$$

Hence the marginal posterior of this hierarchical model is equal to the profiled posterior distribution, the Bayesian analogue of the profile likelihood. Equation (2.14) shows that for the profiled posterior distribution a rather restrictive prior is used: the parameter  $\theta_i$  is acting as the hyper-parameter, and we have a rigid dependence of the parameters  $\Theta_{j|i}$  on the parameter of interest  $\theta_i$  through the mapping  $\mathbf{t}_{j|i}(\cdot)$  as given in equation (2.5).

## 3 Example Distributions

We illustrate the effect of profiling the posterior with several two-dimensional examples and compare the profiled posterior to the marginal posterior distribution.

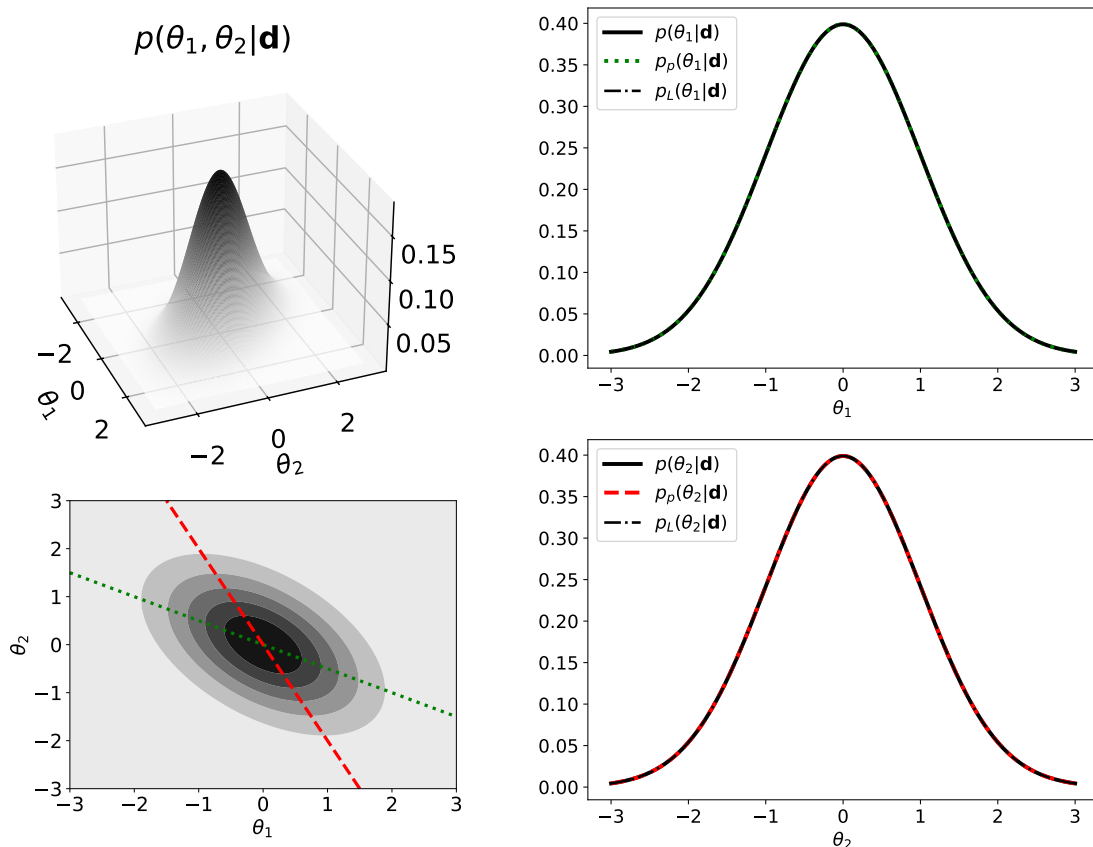


**Figure 1.** On the left, the two-dimensional Gaussian posterior  $p(\theta_1, \theta_2 | \mathbf{d})$  from Eqn. (3.1) is shown with correlation coefficient  $\rho = -0.5$ . In the contour plot, we also show the profiling graphs  $(\theta_1, \mathbf{t}_{1|}(\theta_1))$  (green dotted) and  $(\mathbf{t}_{2|}(\theta_2), \theta_2)$  (red dashed). On the right on top, we compare the marginal  $p(\theta_1 | \mathbf{d})$  to the profiled posterior  $p_p(\theta_1 | \mathbf{d})$ . On the right, at the bottom, we compare the marginal  $p(\theta_2 | \mathbf{d})$  with the profiled posterior  $p_p(\theta_2 | \mathbf{d})$ . In both cases, the marginal and the profiled posterior distribution overlap. Also the Laplace approximations  $p_L(\theta_i | \mathbf{d})$  are indistinguishable from the corresponding marginal distributions.

### 3.1 A Gaussian Distribution

As a first simple case, we consider a posterior distribution of the parameters  $\theta_1$  and  $\theta_2$  given by a two-dimensional Gaussian distribution

$$p(\theta_1, \theta_2 | \mathbf{d}) = \frac{1}{2\pi\sqrt{1-\rho^2}} \exp\left(-\frac{1}{2(1-\rho^2)} (\theta_1^2 - 2\rho\theta_1\theta_2 + \theta_2^2)\right), \quad (3.1)$$

with unit variance and correlation coefficient  $\rho$ . Envision this as a posterior built from a Gaussian likelihood together with a flat prior. Hence including  $\mathbf{d}$  in the equation above is meant as a reminder that the posterior is constructed from a model for the data using a likelihood.

We calculate the marginal posterior distributions  $p(\theta_1 | \mathbf{d})$ ,  $p(\theta_2 | \mathbf{d})$  according to Eqn. (2.2) and the profiled posteriors  $p_p(\theta_1 | \mathbf{d})$ ,  $p_p(\theta_2 | \mathbf{d})$  from Eqn. (2.8). The marginal distributions of a two-dimensional Gaussian are one-dimensional Gaussians, and as can be seen from figure 1, the profiled posterior distributions are identical to these Gaussian marginal distributions.

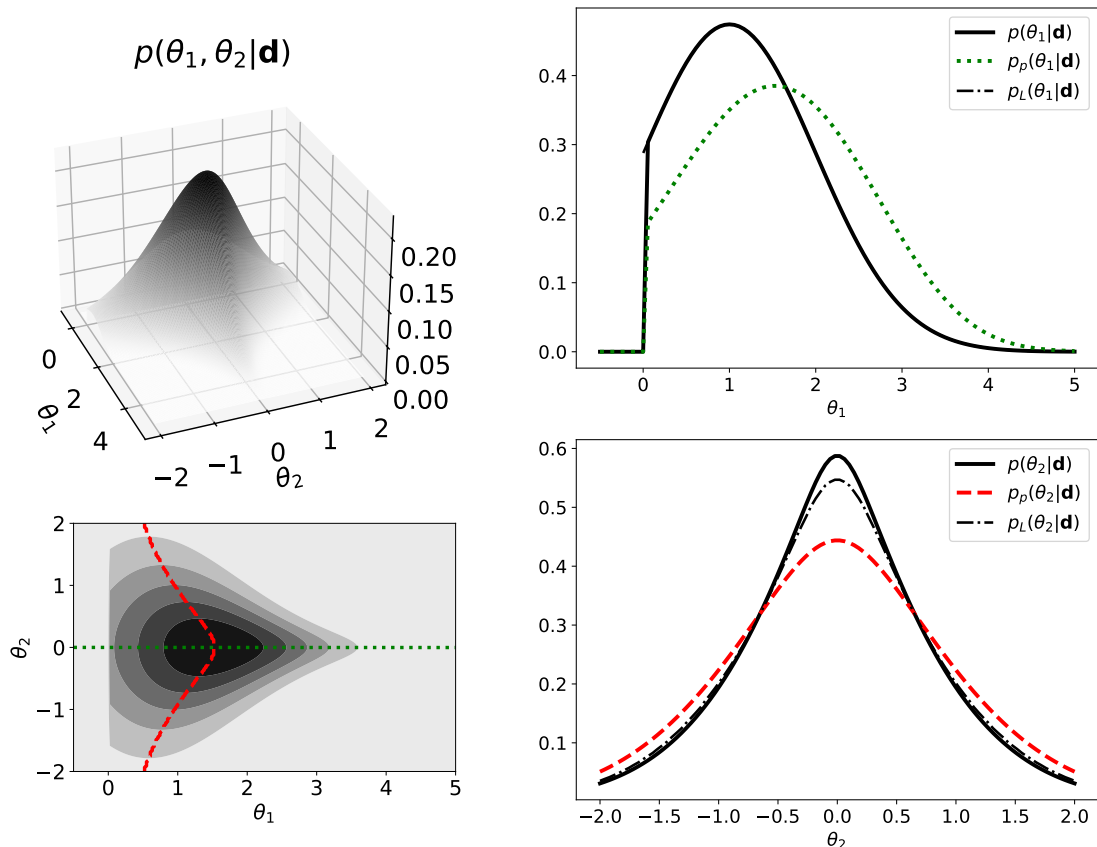


**Figure 2.** On the left, the two-dimensional posterior  $p(\theta_1, \theta_2 | \mathbf{d})$  is shown for the example illustrating the volume effect with  $b = 0.2$  (see Eqn. (3.3)). In the contour plot, we also show the profiling graphs  $(\theta_1, \mathbf{t}_{1|}(\theta_1))$  (green dotted) and  $(\mathbf{t}_{2|}(\theta_2), \theta_2)$  (red dashed). On the right on top, we compare the marginal  $p(\theta_1 | \mathbf{d})$  to the profiled posterior  $p_p(\theta_1 | \mathbf{d})$ . On the right, at the bottom, we compare the marginal  $p(\theta_2 | \mathbf{d})$  with the profiled posterior  $p_p(\theta_2 | \mathbf{d})$ . The corresponding Laplace approximations  $p_L(\theta_i | \mathbf{d})$  are shown as dashed-dotted lines.

To calculate the Laplace approximation we determine the  $\mathcal{F}$  from Eqn. (2.11) with finite differences followed by a Richardson extrapolation as provided by numdifftools [20]. For this Gaussian example a numerical approximation would not have been necessary, but we will follow this numerical scheme also for the following more complicated examples. Clearly, the Laplace approximation Eqn. (2.12) is exact for a Gaussian as can be also seen from figure 1.

The profiled posterior distribution is the distribution of one parameter, given that the other parameter is following this profiling graph (see Eqn. (2.15)). Both profiling graphs are straight lines. The  $\mathbf{t}_{1|}$  maps each  $\theta_1$  to a  $\theta_2 = \mathbf{t}_{1|}(\theta_1)$ , and the profiling graph consists out of these points  $(\theta_1, \theta_2 = \mathbf{t}_{1|}(\theta_1))$ . Similarly, for the profiling graph  $(\mathbf{t}_{2|}(\theta_2), \theta_2)$ , each  $\theta_2$  is mapped to a  $\theta_1 = \mathbf{t}_{2|}(\theta_2)$ .

### 3.2 A model for the volume effect

The following construction mimics the situation in cosmological parameter estimation if our cosmological model B is an extension of the reference model A but with two additional parameters. Model A is determined by the parameters,  $\boldsymbol{\alpha}$  which we will not consider further. In addition, to these parameters, model B has two further parameters  $\theta_1 \geq 0$  and  $\theta_2$ . For

$\theta_1 = 0$  model B turns into model A. The volume effect in such a nested model can be described in the following way: When the parameter  $\theta_1$  approaches zero the model B reduces to model A, and in this limit the other parameter  $\theta_2$  of model B is less constrained. This leads to an increased volume in the parameter space for model A, which could drive the posterior towards low values of  $\theta_1$  upon marginalisation. See also Herold & Ferreira [21] in their presentation of the volume effect for the early dark energy model.

We construct the following model showing the traits of the volume effect as described above. The distribution of the parameter  $\theta_1 \geq 0$  is assumed to be a truncated Gaussian with mean  $a$  and variance  $\sigma_1^2$ :

$$q_1(\theta_1) = C \exp\left(-\frac{(\theta_1 - a)^2}{2\sigma_1^2}\right) \text{ for } \theta_1 > 0 \quad (3.2)$$

and  $q_1(\theta_1) = 0$  for  $\theta_1 \leq 0$ . The normalisation is  $1/C = \int_0^\infty \exp\left(-\frac{(\theta_1 - a)^2}{2\sigma_1^2}\right) d\theta_1$ . The distribution of the parameter  $\theta_2$  is again a Gaussian with variance  $\sigma_2^2$ . For large  $\theta_1 \gg 0$  we assume a constant  $\sigma_2 \approx v$  corresponding to a finite resolution of the measurement or observations. For small  $\theta_1$  the distribution of  $\theta_2$  should broaden. We model this behaviour with

$$q_2(\theta_2|\theta_1) = \frac{1}{\sigma_2\sqrt{2\pi}} \exp\left(-\frac{\theta_2^2}{2\sigma_2^2}\right) \quad \text{and} \quad \sigma_2 = \exp(-b\theta_1^2) + v. \quad (3.3)$$

Now the likelihood can be written as

$$\mathcal{L}(\mathbf{d}|\theta_1, \theta_2) = q_2(\theta_2|\theta_1) q_1(\theta_1). \quad (3.4)$$

Comparing Eqn. (3.4) to Eqn. (3.6) from the next section, we realise that this example is closely related to the ridge example of Berger et al. [22]. For another model illustrating the volume effect, see [11].

To detail our example further, we assume  $a = 1$ ,  $\sigma_1 = 1$ , and  $v = 0.1$ ,  $b = 0.2$ . We want to compare a well-defined profiled posterior to the profile likelihood, therefore we have to use a flat prior restricted to a finite parameter domain. In the following, we choose  $\theta_1 \in A_1 = [0, 8]$  and  $\theta_2 \in A_2 = [-5, 5]$ . The posterior is then  $p(\theta_1, \theta_2|\mathbf{d}) \propto \mathcal{L}(\mathbf{d}|\theta_1, \theta_2)\mathbb{1}_{A_1}(\theta_1)\mathbb{1}_{A_2}(\theta_2)$  (with  $\mathbb{1}_A(x) = 1$  if  $x \in A$  and zero otherwise). For each  $\theta_1$ , we determine the function  $r(\theta_1) = \max_{\theta_2} p(\theta_1, \theta_2|\mathbf{d})$  by numerical maximisation. Then we determine the normalisation  $c_1 = \int_{A_1} r(\theta_1)d\theta_1$  by a numerical integration and finally obtain

$$p_p(\theta_1|\mathbf{d}) = \frac{1}{c_1} \max_{\theta_2} p(\theta_1, \theta_2|\mathbf{d}). \quad (3.5)$$

We proceed similarly for  $p_p(\theta_2|\mathbf{d})$ . With a numerical integration of Eqn. (3.4) we determine the marginal posterior distributions according to Eqn. (2.2).

In figure 2 the bulge for small  $\theta_1$  is clearly visible in the two-dimensional distribution  $p(\theta_1, \theta_2|\mathbf{d})$ . Due to the mirror symmetry the profiling graph,  $(\theta_1, \mathbf{t}_{1|}(\theta_1) = 0)$  is a straight line, whereas the profiling graph  $(\mathbf{t}_{2|}(\theta_2), \theta_2)$  is showing a dent. The profiled posterior and marginal posterior distributions for  $\theta_2$  are symmetric around the same maximum, but the marginal posterior is more strongly peaked. For  $\theta_1$  the profiled posterior is showing a significant shift towards large values. The maximum of the marginal posterior is at  $\theta_1 = 1$  but the maximum of the profiled posterior is at the larger value  $\theta_1 = 1.67$ . Also, the marginal posterior distribution has significantly more weight for smaller values of  $\theta_1$  than the profiled posterior distribution.

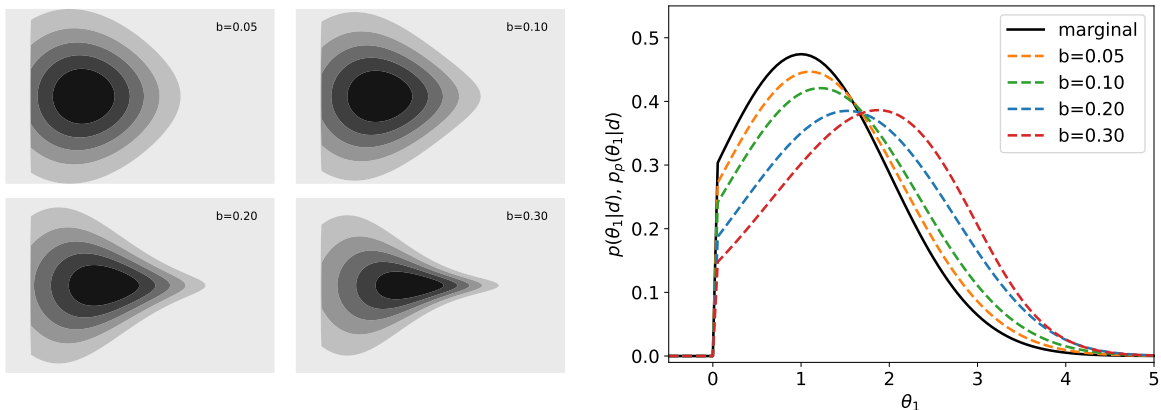


**Figure 3.** The contour plots on the left show the  $p(\theta_1, \theta_2 | \mathbf{d})$  for several values for  $b$  (compare also with figure 2). In the right plot the marginal posterior  $p(\theta_1 | \mathbf{d})$  (solid black line) and the profiled posterior distributions  $p_p(\theta_1 | \mathbf{d})$  (dashed lines) are shown for a varying factor  $b$  according to Eqn.(3.3). The marginal is invariant under changes of  $b$ .

This behaviour is called the "volume effect". For a fixed  $\theta_1$  the likelihood (3.4) is a Gaussian in  $\theta_2$  and consequently the  $p_L(\theta_1 | \mathbf{d})$  is giving the exact value for the marginal  $p(\theta_1 | \mathbf{d})$ . For  $\theta_2$  the Laplace approximation  $p_L(\theta_2 | \mathbf{d})$  is slightly broader than the marginal.

With the factor  $b$  in Eqn. (3.3) we specify how strongly the variance of the parameter  $\theta_2$  depends on the parameter  $\theta_1$ . In this way, we obtain a model with a tuneable volume effect. Figure 3 shows the marginal  $p(\theta_2 | \mathbf{d})$  and the profiled posterior distribution  $p_p(\theta_2 | \mathbf{d})$  for a series of values for  $b$ . The marginal posterior distribution is independent of the value of  $b$ , whereas the profiled posterior distribution is strongly depending on the value of  $b$ . For small  $b$  the profiled posterior is approaching the marginal posterior distribution, but for larger  $b$  we generate a strong "volume effect" and the profiled posterior distribution is shifted towards larger values for  $\theta_1$ . Similarly, we considered a variable  $v$  in Eqn.,(3.3) for a fixed  $b$ . In this way, we investigate how the resolution of the measurements influences the distribution. Essentially, the same picture as in figure 3 emerges: the marginal posterior distribution  $p(\theta_2 | \mathbf{d})$  does not depend on the value of  $v$ , while the profiled posterior distribution  $p_p(\theta_2 | \mathbf{d})$  is strongly dependent on  $v$ . For large  $v$  the profiled posterior approaches the marginal posterior distribution

In this model, we may tune the volume effect or the resolution. In a typical situation of parameter estimation, both are fixed by the experimental setup. Hence, it seems advisable to use the marginal posterior distribution if one wants to get results independent of the resolution or the details of a volume effect.

### 3.3 A model with a ridge

Berger et al. [22] discuss with several examples why an integrated (marginalised) likelihood should be preferred over a profile likelihood. Here we give a slightly simplified version<sup>1</sup> of their example 3. Our model from the last section is closely related to this ridge model. We present the construction of this model in some detail, since it allows us to show that the resulting likelihood is not an ad hoc structure. Consider two measurements modelled with two independent random variables  $X$  and  $Y$ , where  $X \sim N(\theta_1, 1)$  follows a normal

<sup>1</sup>To make the connection with Berger et al. [22] use  $n = 1$  and  $\theta_2 = \lambda$  in their Eqn. (11), (12), and (13).

distribution with mean  $\theta_1$  and unit variance, and  $Y \sim N(\theta_2, \exp(-\theta_1^2))$  with mean  $\theta_2$  and variance that depends on  $\theta_1$  exponentially. The likelihood can be obtained by multiplying the two Gaussians resulting in

$$\begin{aligned} \mathcal{L}(\mathbf{d}|\theta_1, \theta_2) &= \frac{1}{\sqrt{2\pi}} \exp\left(-\frac{1}{2}(x - \theta_1)^2\right) \frac{1}{\sqrt{2\pi \exp(-\theta_1^2)}} \exp\left(-\frac{(y - \theta_2)^2}{2 \exp(-\theta_1^2)}\right) \\ &= \frac{1}{2\pi} \exp\left(-\frac{1}{2}(x^2 - 2x\theta_1) - \frac{(y - \theta_2)^2}{2 \exp(-\theta_1^2)}\right). \end{aligned} \quad (3.6)$$

The data  $\mathbf{d} = (x, y)$  consists out of the two measured values  $x$  and  $y$ . The conditional maximum likelihood estimate for  $\theta_2$  is  $\tilde{\theta}_2 = y$  for each  $\theta_1$ , therefore, the profile likelihood for  $\theta_1$  is  $\mathcal{L}_p(\theta_1) \propto \exp(x\theta_1)$  (see Berger et al. [22]). Depending on the sign of the measured value  $x$ , this profile likelihood  $\mathcal{L}_p(\theta_1)$  is exponentially divergent for  $\theta_1 > 0$  if  $x > 0$  (or for  $\theta_1 < 0$  if  $x < 0$ ). However, a marginalised likelihood reads  $p(\theta_1|\mathbf{d}) \propto \exp(-\frac{1}{2}(x - \theta_1)^2)$  providing some localisation in parameter space.

To concretise, we assume that we observed  $x = 1$  and  $y = 0$ , hence  $\mathbf{d} = (1, 0)$ . As above we use a flat prior restricted to a finite parameter domain. In the following, we choose  $\theta_1 \in A_1 = [-1, 1]$  and  $\theta_2 \in A_2 = [-1, 4]$ . The posterior is then  $p(\theta_1, \theta_2|\mathbf{d}) \propto \mathcal{L}(\mathbf{d}|\theta_1, \theta_2)\mathbb{1}_{A_1}(\theta_1)\mathbb{1}_{A_2}(\theta_2)$  (with  $\mathbb{1}_A(x) = 1$  if  $x \in A$  and zero otherwise). We calculate the profiled and marginal posterior distributions as explained in section 3.2. In figure 4 the ridge is clearly visible in the distribution of the parameters. Due to the mirror symmetry the profiling graph,  $(\theta_1, \mathbf{t}_{1|}(\theta_1) = 0)$  is a straight line following this ridge, whereas the profiling graph  $(\mathbf{t}_{2|}(\theta_2), \theta_2)$  is showing a cusp. The profiled posterior and marginal posterior distribution for  $\theta_2$  overlap, but for  $\theta_1$  they show a qualitatively different behaviour. The Laplace approximation follows the marginal  $p(\theta_2|\mathbf{d})$  closely, for  $\theta_1$  we observe a shift. As already discussed the profile likelihood  $\mathcal{L}_p(\theta_1)$  is divergent. This is reflected in the behaviour of the profiled posterior  $p_p(\theta_1|\mathbf{d})$  with its peak at the boundary. The marginalisation of the posterior distribution is able to regularise this divergence and we obtain a bell-shaped marginal posterior distribution  $p(\theta_1|\mathbf{d})$  with a mode only slightly larger than the measured  $x = 1$ .

Montoya et al. [23] argue that example 3 from Berger et al. [22] (our  $\mathcal{L}(\mathbf{d}|\theta_1, \theta_2)$  from Eqn. (3.6)) is not a valid likelihood function because it does not include the effect of a finite precision of the measurements. We investigate this by adding a constant  $v$  to the variance of  $y$ , similar to the constant component in  $\sigma_2$  in Eqn. (3.4). Now for a finite precision  $v$  the criticism of Montoya et al. [23] does not apply anymore. Still the profiled posterior distribution is approaching the distribution with a peak at the boundary, for small  $v$ . Similarly to the example in section 3.2 the profiled posterior distribution is strongly depending on the resolution  $v$ , whereas again the marginal posterior distribution stays invariant.

Sometimes the volume effect is mentioned as reason why a profile likelihood should be used instead of the marginal posterior distribution. However, in this case only the marginalisation (the "volume" integration) leads to a well-behaved distribution for  $\theta_1$ , whereas the maximisation results in an almost singular profiled posterior distribution.

### 3.4 A Rosenbrock function

Often the Rosenbrock function [24] is used to illustrate convergence properties of Markov chain Monte Carlo strategies (e.g. [25]). We use a similarly transformed Gaussian as our parameterisation of such a "banana-shaped" distribution [26]. The posterior  $p(\theta_1, \theta_2|\mathbf{d})$  is

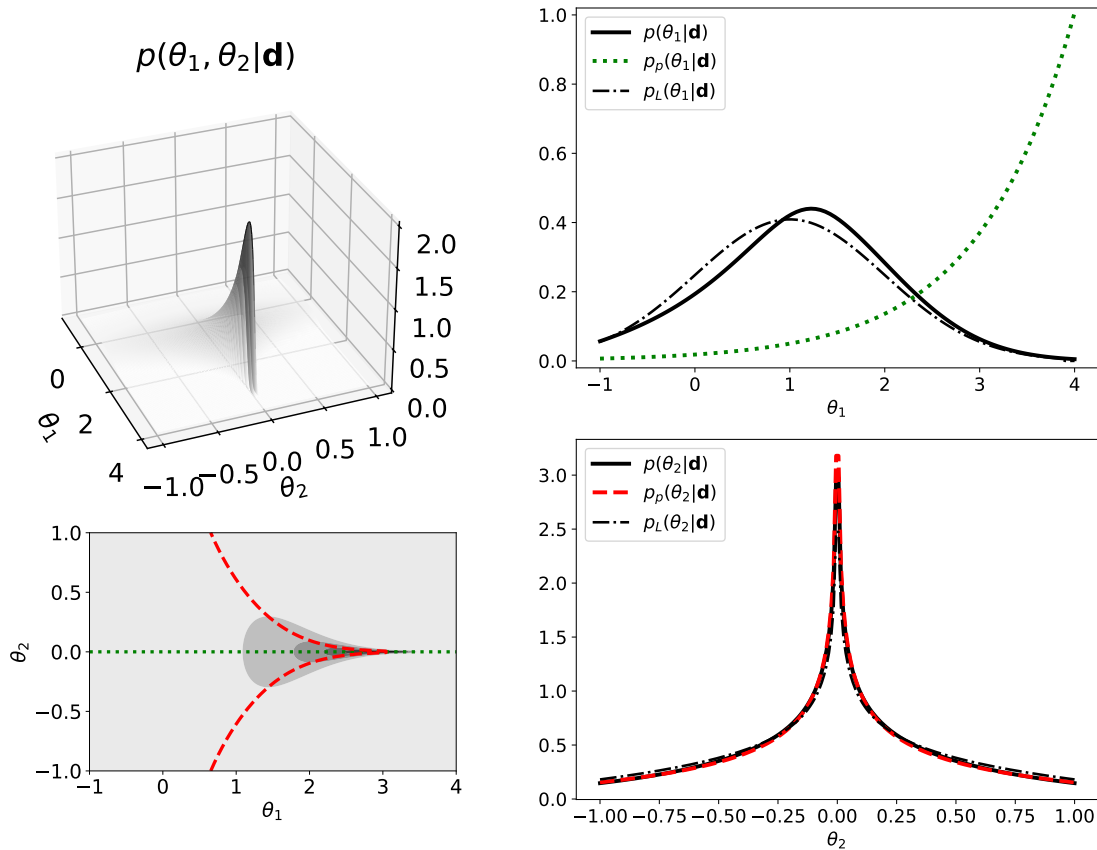


**Figure 4.** On the left, the two-dimensional posterior  $p(\theta_1, \theta_2 | \mathbf{d})$  is shown for the ridge example. In the contour plot, we also show the profiling graphs  $(\theta_1, \mathbf{t}_{j1}(\theta_1))$  (green dotted) and  $(\mathbf{t}_{j2}(\theta_2), \theta_2)$  (red dashed). On the right on top, we compare the marginal  $p(\theta_1 | \mathbf{d})$  to the profiled posterior  $p_p(\theta_1 | \mathbf{d})$ . On the right, at the bottom, we compare the marginal  $p(\theta_2 | \mathbf{d})$  with the profiled posterior  $p_p(\theta_2 | \mathbf{d})$ . The corresponding Laplace approximations  $p_L(\theta_i | \mathbf{d})$  are shown as dashed-dotted lines.

now proportional to

$$p(\theta_1, \theta_2 | \mathbf{d}) \propto \exp \left[ -\frac{1}{2(1-\rho^2)} \left( \frac{\theta_1^2}{a^2} + a^2 t^2 - 2\rho\theta_1 t \right) \right], \quad (3.7)$$

with  $t = \theta_2 - \frac{b}{a^2}\theta_1^2 - ba^2$ , the parameters  $a, b \in \mathbb{R}$ , and the correlation coefficient  $\rho$ . We calculate the marginal and the profiled posterior distributions as described for the example in section 3.2. In figure 5 we show a slightly asymmetric distribution  $p(\theta_1, \theta_2 | \mathbf{d})$  obtained by using the parameters  $a = 1.2$ ,  $b = 2$ , and the correlation coefficient  $\rho = 0.9$ . For  $\theta_1$  the marginal distribution  $p(\theta_1 | \mathbf{d})$  shows a bell shaped curve, matched by the profiled posterior  $p_p(\theta_1 | \mathbf{d})$ . For  $\theta_2$  the marginal distribution  $p(\theta_2 | \mathbf{d})$  is clearly skewed but the profiled posterior  $p_p(\theta_2 | \mathbf{d})$  shows an even stronger skewing with a heavy tail for large  $\theta_2$ . This is also the direction where the credibility region of the Rosenbrock function is curved inward (concave). The difference between the profiled posterior and marginal posterior is not astonishing if one is looking at the profiling graph. The profiling graph  $(\mathbf{t}_{j2}(\theta_2), \theta_2)$  is following only one "branch" in the posterior distribution, whereas the marginal posterior incorporates contributions from both branches. The Laplace approximation is almost perfect for the marginal posterior  $p(\theta_1 | \mathbf{d})$ . However for  $\theta_2$  the Laplace approximation  $p_L(\theta_2 | \mathbf{d})$  is missing the contribution from the

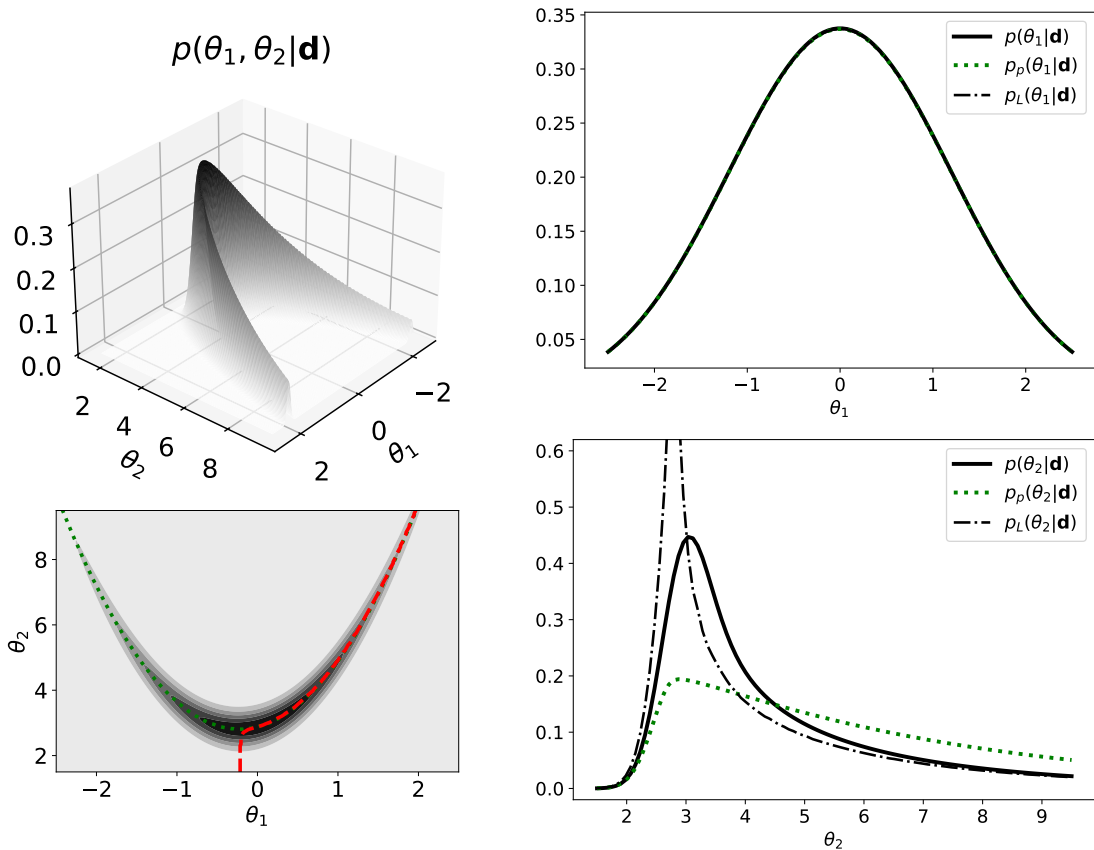


**Figure 5.** On the left, the "banana-shaped" two-dimensional posterior  $p(\theta_1, \theta_2 | \mathbf{d})$  is shown for the Rosenbrock example. In the contour plot, we also show the profiling graphs  $(\theta_1, \mathbf{t}_{1|}(\theta_1))$  (green dotted) and  $(\mathbf{t}_{2|}(\theta_2), \theta_2)$  (red dashed). On the right on top, we compare the marginal  $p(\theta_1 | \mathbf{d})$  to the profiled posterior  $p_p(\theta_1 | \mathbf{d})$ . On the right, at the bottom, we compare the marginal  $p(\theta_2 | \mathbf{d})$  with the profiled posterior  $p_p(\theta_2 | \mathbf{d})$ . The corresponding Laplace approximations  $p_L(\theta_i | \mathbf{d})$  are shown as dashed-dotted lines.

second branch of the posterior and is therefore shifted and significantly tighter than the full marginal. We checked with the hybrid Rosenbrock function of Pagani et al. [27] that also in higher dimensions the profiled posteriors differ from the marginal posterior distributions.

### 3.4.1 A Rosenbrock distribution with added noise

With this Rosenbrock function, we can illustrate a further characteristic trait of the profiling procedure. Up to now, we considered smooth posteriors in our examples. Since the likelihood and consequently the posterior distributions are depending on the actual data they often exhibit a more bumpy shape. We emulate this by adding noise to the posterior (3.7) and re-normalise the distribution. Compare the posterior without noise in figure 5 to the posterior with noise in figure 6. The overall characteristics of the one-dimensional marginal and profiled posterior distributions do not change significantly by adding the noise. In addition, the profiling graph  $(\theta_1, \mathbf{t}_{1|}(\theta_1))$  for  $\theta_1$  only shows small wiggles in the noisy case. But the profiling graph  $(\mathbf{t}_{2|}(\theta_2), \theta_2)$  for  $\theta_2$  is not continuous any more. It jumps from one branch to the other and back (see figure 6). In the following analysis of the supernova data we observe a similar behaviour. The Laplace approximations show the same overall characteristics as

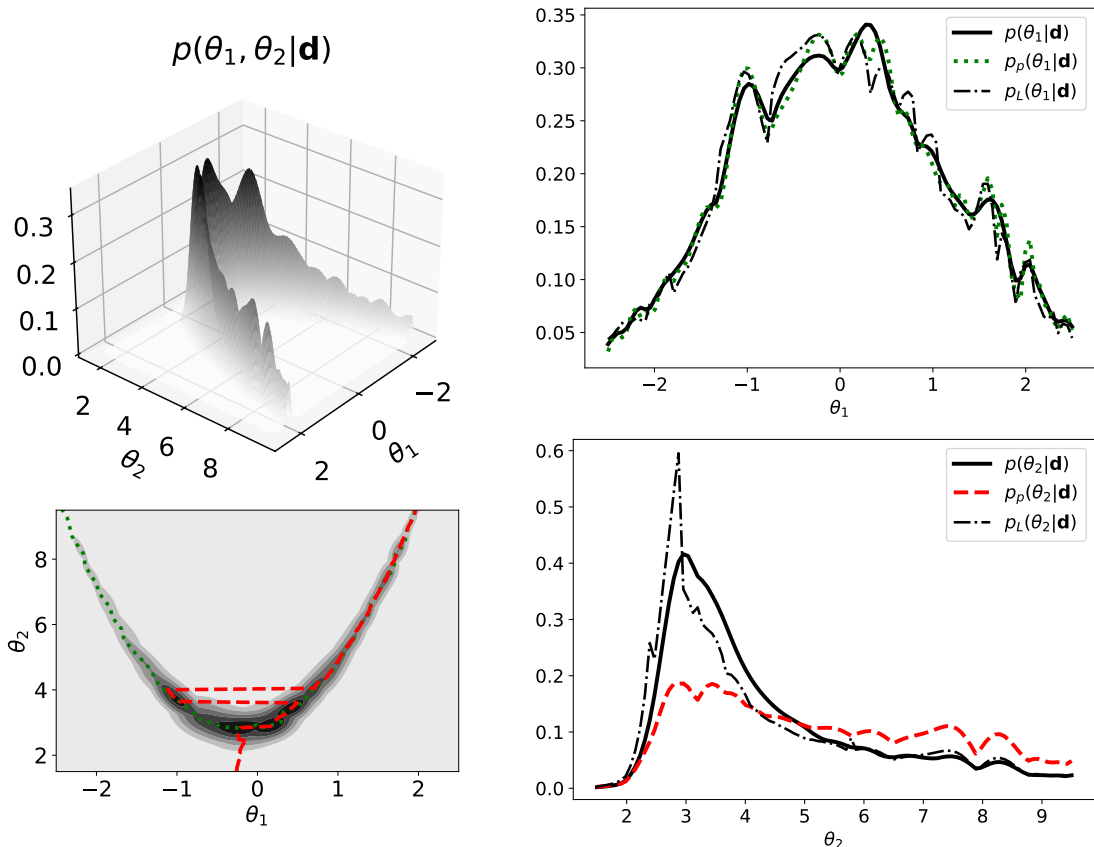


**Figure 6.** Similar plots as in figure 5 but with added noise.

for the example without noise. Furthermore the jumps in the profiling path bring about discontinuities in the Laplace approximations  $p_L(\theta_2|\mathbf{d})$ . We will see this effect even more pronounced in the analysis of real data.

## 4 Cosmological parameters from the SN Ia magnitude redshift relation

The physical foundation of the following analysis is that type Ia supernova explosions essentially have the same peak luminosity. Measurement of the magnitude and the redshift of such an explosion gives information about the geometry of spacetime between our position and the supernova. This can be used to constrain parameters of cosmological models for the spacetime. For more information on the method and on the history of this approach see the review by S. Perlmutter [28]. In the following we use the Pantheon+ supernova data set [15]. Partly we redo the analysis of Brout et al. [29]. We confirm their results in the cases where we investigate the same situations. Additionally we focus on the comparison between the marginal posterior and the profiled posterior distribution.

### 4.1 The sample, the models and the analysis

The Pantheon+ data set<sup>2</sup> [15] includes the redshift  $z_i$  and the distance modulus  $\mu_i$  of  $N = 1701$  type Ia supernovae. We use supernovae with a redshift of  $z > 0.01$ , hence we are left with 1590

<sup>2</sup>The data is easily accessible at <https://github.com/PantheonPlusSH0ES/DataRelease>.

**Table 1.** The cosmological models, their parameters and the priors used for the MCMC calculations.  $\mathcal{U}(a, b)$  is the flat / uniform distribution on the interval  $[a, b]$ .

cosmology	priors
flat $w$ CDM	$H_0 \sim \mathcal{U}(10, 200)$ , $\Omega_m \sim \mathcal{U}(0.05, 1)$ , $\Omega_\Lambda = 1 - \Omega_m$ , $w \sim \mathcal{U}(-3, 1)$
non-flat $\Lambda$ CDM	$H_0 \sim \mathcal{U}(10, 200)$ , $\Omega_m \sim \mathcal{U}(0.05, 1.5)$ , $\Omega_\Lambda \sim \mathcal{U}(0, 1.5)$ , $w = -1$
non-flat $w$ CDM	$H_0 \sim \mathcal{U}(10, 200)$ , $\Omega_m \sim \mathcal{U}(0.05, 1.5)$ , $\Omega_\Lambda \sim \mathcal{U}(0, 1.5)$ , $w \sim \mathcal{U}(-3, 1)$

data points. To compare the corrected and standardised distance moduli from the Pantheon+ sample with the theoretical predictions, we assume a Gaussian likelihood where we use the provided covariance matrix  $\Sigma$  including systematic and statistical correlations. Then the likelihood is

$$\mathcal{L}(\mathbf{d} | \Theta) = \frac{1}{((2\pi)^N \det(\Sigma))^{\frac{1}{2}}} \exp \left[ -\frac{1}{2} \mathbf{\Delta}_\mu(\Theta)^T \Sigma^{-1} \mathbf{\Delta}_\mu(\Theta) \right]. \quad (4.1)$$

$\mu_{\text{model}}(z, \Theta)$  is the predicted distance modulus at redshift  $z$  for a given model with parameters  $\Theta$ , and the  $\mathbf{\Delta}_\mu(\Theta) = (\mu_{\text{model}}(z_1, \Theta) - \mu_1, \dots, \mu_{\text{model}}(z_N, \Theta) - \mu_N)^T$ . Assuming a Friedman-Lemaitre-Robertson-Walker metric we can calculate a theoretical prediction for the distance moduli for given redshifts in several different cosmological models. As parameters  $\Theta$  we consider the matter content  $\Omega_m$ , the Hubble parameter  $H_0$ , and depending on the extension of the model, also the dark energy contribution  $\Omega_\Lambda$  and the equation of state parameter  $w$  for the dark energy component. To numerically determine the distance modulus we use the tools provided in Astropy [30]. We fix the following parameters to the values determined in the Planck 18 analysis [31]:  $T_{\text{CMB}} = 2.7255\text{K}$ ,  $N_{\text{eff}} = 3.046$ ,  $m_\nu = 0.06\text{eV}$  (for one neutrino species, the others are assumed mass-less). The mass parameter  $\Omega_m = \Omega_b + \Omega_{\text{DM}}$  includes the contribution from baryons  $\Omega_b = 0.04897$  and dark matter  $\Omega_{\text{DM}}$ . The properties of the cosmological models are summarised in table 1. We choose these flat priors since we want to make the connection with the profile likelihood as described in section 2. For the flat  $w$ CDM model we have  $\Omega_m + \Omega_\Lambda = 1$  and for the non-flat  $\Lambda$ CDM model we have a fixed  $w = -1$ . In the non flat  $w$ CDM and  $\Lambda$ CDM models  $\Omega_m$  and  $\Omega_\Lambda$  may vary independently.

The posterior distributions of  $H_0$ ,  $\Omega_m$ ,  $\Omega_\Lambda$ , and  $w$  are estimated using Monte Carlo Markov chain calculations. These Markov chains are generated with the affine invariant ensemble sampler emcee [32]. We use 10 parallel chains with at least 1 Mio. up to 20 Mio. of steps. After visual inspection with a trace-plot we discard the burnin phase. We made sure that the effective sample size (see e.g. [33]) was always larger than  $10^4$ . For the improved convergence criterion  $\hat{R}$  [33] we have  $\hat{R} - 1 \leq 0.01$  for any of the parameters and for all the models considered. This is an indication for well converged chains. The marginal distributions are estimated from these Markov chains using a kernel density estimate.

To obtain the profiled posteriors we use the downhill simplex minimiser provided in SciPy [34]. In the minimisation we use boundaries given by the limits of the uniform priors as shown in table 1. To verify that we locate the global maxima, we inspect the graphs visually and compare with the results from a simulated annealing strategy. For the non-flat  $w$ CDM model we use a brute force grid-search followed by a downhill simplex algorithm. Especially for a non-flat  $w$ CDM model we observe parameter combinations without big bang singularity [35]. In such situations the integration used to determine the distance moduli is

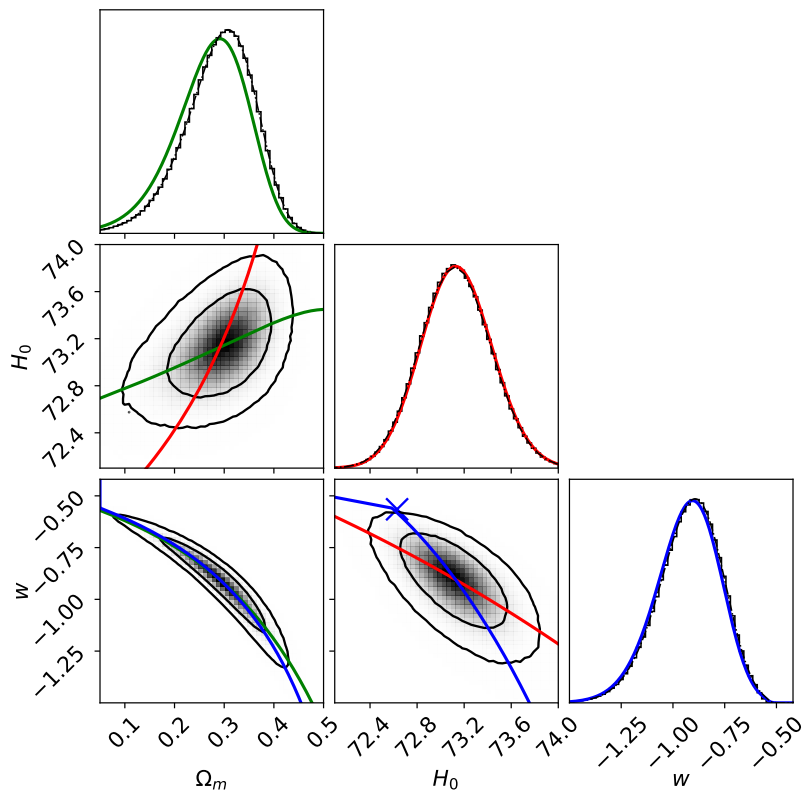


**Figure 7.** The distribution of the cosmological parameters for the flat  $w$ CDM model. Marginal distributions are solid black. The profiled posterior distributions and the profile graph for  $\Omega_m$  are in green, for  $H_0$  in red, and for  $w_0$  in blue. The Laplace approximations are overlapping with the exact marginal posterior distributions. The kink in the profiling graph, due to the border  $\Omega_m \geq 0.05$ , is marked with an  $\times$ .

not converging. We use this as a criterion to exclude these parameter combinations and set the corresponding likelihood to zero (see also [36]).

## 4.2 Marginal and profiled posterior distribution of the parameters

Figures 7, 8, and 9 show the one- and two-dimensional marginal posterior distributions of the cosmological parameters obtained for our models, together with the one-dimensional profiled posterior distributions and the profiling graphs. The two contour levels shown in the figures are the highest density credible regions that include 68% and 95% of the posterior mass. From the marginal posterior distribution, we confirm the estimates of the cosmological parameters as given in table 3 of Brout et al. [29] for the flat  $\Lambda$ CDM (not shown here), the flat  $w$ CDM and the non-flat  $\Lambda$ CDM models (compare also with figure 9 from Brout et al. [29]). A discussion of these results and their implications for cosmology are given in Brout et al. [29]. Here we compare the marginal with the profiled posterior distributions.

### 4.2.1 Flat $w$ CDM and non-flat $\Lambda$ CDM

As can be seen in the figures 7 and 8 the profiled posterior and the marginal posterior distributions are almost identical for the flat  $w$ CDM model and the non-flat  $\Lambda$ CDM model.

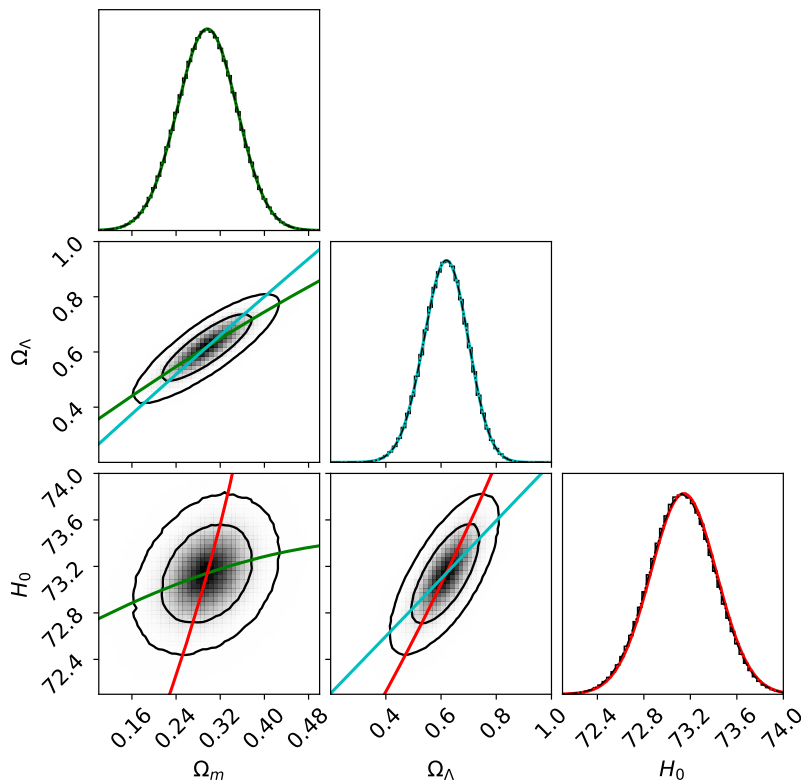


**Figure 8.** The distribution of the cosmological parameters for the non-flat  $\Lambda$ CDM model. Marginal distributions are solid black. The profiled posterior distribution and the profiling graph for  $\Omega_m$  is in green, for  $H_0$  in red, and for  $\Omega_\Lambda$  in cyan. The Laplace approximations are overlapping with the exact marginal posterior distributions.

Only in the  $w$ CDM model we observe a shift towards lower values for  $\Omega_m$  in the profiled posterior distribution  $p_p(\Omega_m|\mathbf{d})$  in comparison to the marginal posterior distribution  $p(\Omega_m|\mathbf{d})$ . As expected from the example in section 3.4 we observe a non-convex credible region in the two-dimensional marginal posterior for  $\Omega_m$  and  $w$ . For the other parameters, the profiled and marginal distributions overlap, and also the credible regions are convex and almost elliptical. For the flat  $w$ CDM model and the non-flat  $\Lambda$ CDM model the Laplace approximation to the marginal posterior distribution is perfect. Nearly all the profiling graphs for the flat  $w$ CDM model (figure 7) and the non-flat  $\Lambda$ CDM model (figure 8) are smooth curves. Only for the flat  $w$ CDM model we observe a kink in a profiling graph. At this point, the minimiser, used in the profiling procedure, hits the boundary enforcing  $\Omega_m \geq 0.05$ . Because  $\Omega_m$  also includes the baryonic component we do not allow smaller values for  $\Omega_m$ .

#### 4.2.2 Non-flat $w$ CDM

The overall agreement between the profiled and marginal posterior distribution of the cosmological parameters dwindles away when we look at the results from a non-flat  $w$ CDM model in figure 9. Here we are going beyond the analysis presented in Brout et al. [29]. However, the marginal posterior distribution of  $H_0$  is hardly affected by the introduction of additional parameters and is in agreement with the profiled distribution. The marginal posterior dis-

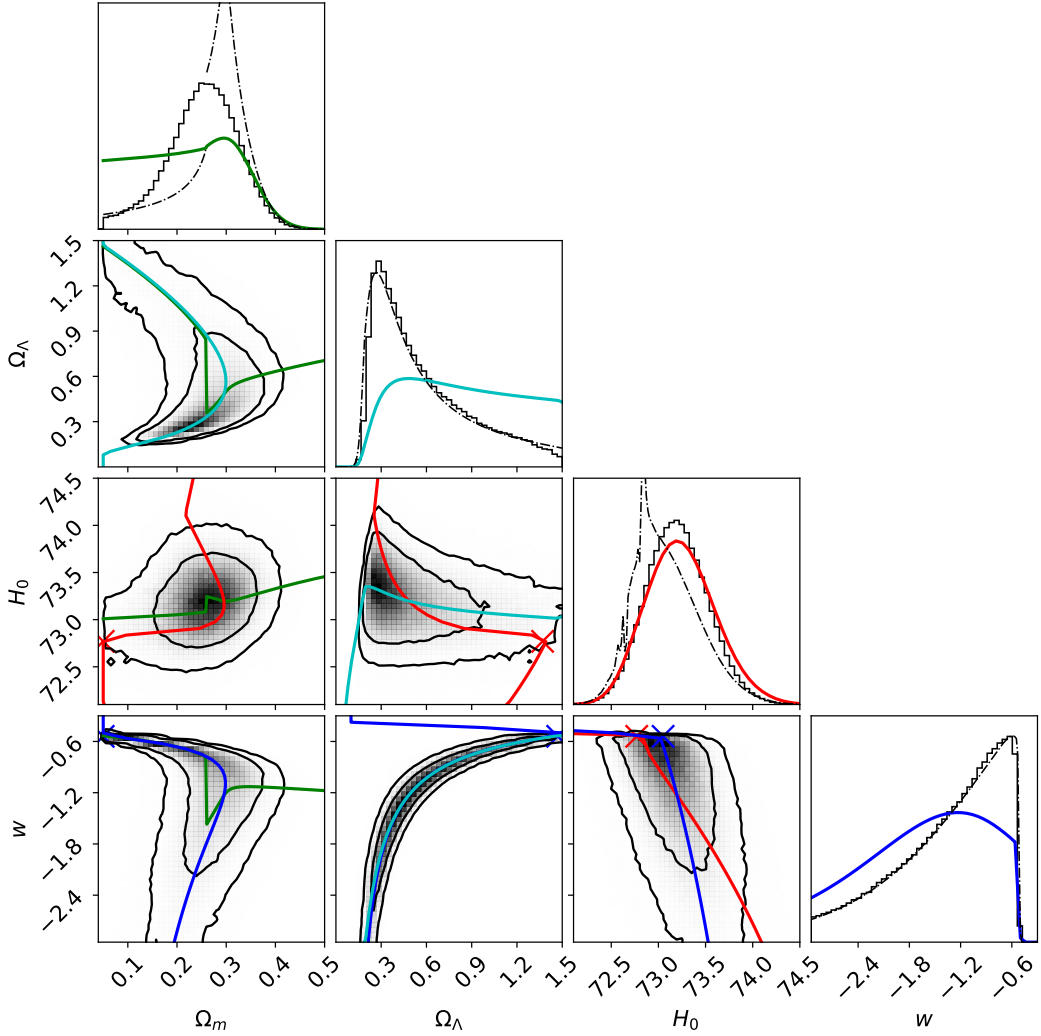


**Figure 9.** The distribution of the cosmological parameters for the non-flat  $w$ CDM model. Marginal distributions are solid black. The profiled posterior distribution and the profiling graph for  $\Omega_m$  are in green, for  $H_0$  in red, for  $w_0$  in blue, and for  $\Omega_\Lambda$  in cyan. The kinks in the profiling graphs, due to the border  $\Omega_m \geq 0.05$ , are marked with  $\times$ -es. The Laplace approximations for the marginal distributions are shown as dashed-dotted lines. The jump in  $p_L(\Omega_m|\mathbf{d})$  is *not* a numerical artefact.

tribution of  $\Omega_m$  is still bell shaped but the marginal posterior distributions of  $\Omega_\Lambda$  and  $w$  are heavily skewed. The marginal posterior distribution of  $w$  peaks at a value greater than  $-1$  but has a significant weight in the region smaller than  $-1$ . For  $\Omega_\Lambda$  values smaller than  $0.5$  are also possible, but still  $\Omega_\Lambda$  is clearly bounded away from zero with almost no weight below a value of  $0.2$ . The two-dimensional marginal posterior distributions of  $\Omega_m-w$ ,  $\Omega_m-\Omega_\Lambda$  and  $\Omega_\Lambda-w$  show distinct non-convex credible regions. As expected from the discussion in section 3.4 the one dimensional profiled posterior distributions for  $\Omega_m$ ,  $\Omega_\Lambda$  and  $w$  show an even stronger skewing than already visible in the corresponding marginal posterior distributions. Indeed, the profiled posterior for  $\Omega_\Lambda$  is an almost flat distribution for  $0.4 < \Omega_\Lambda$  up to and beyond  $1.0$ , offering no further constraints. In addition,  $\Omega_m$  and  $w$  are significantly less constrained

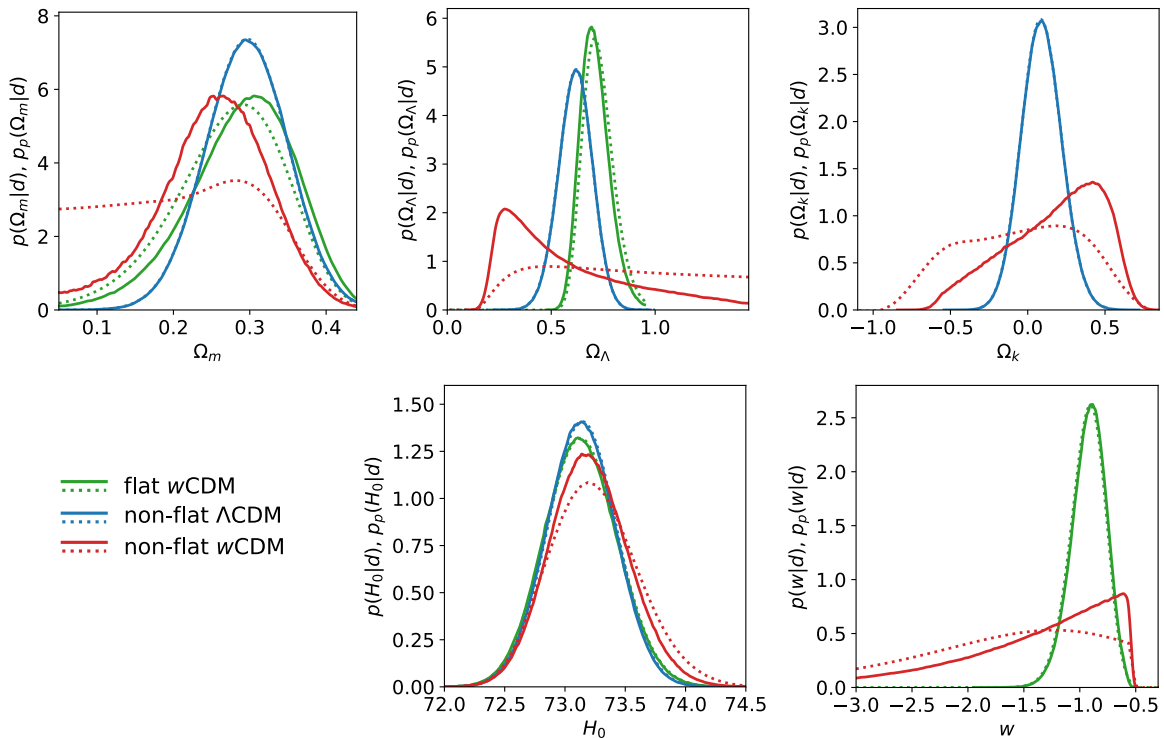


**Figure 10.** Marginal posterior distribution (solid lines) and profiled posterior distributions (dotted lines) for the parameters in all our models.

by the profiled posterior than by the marginal posterior. The profiling graphs in the  $\Omega_m$ – $\Omega_\Lambda$  and  $\Omega_m$ – $w$  contour plots show jumps similar to the jumps in the example from section 3.4. Some of the profiling graphs also show kinks, where the minimiser hits the boundary enforcing  $\Omega_m > 0.05$ . For this non-flat  $w$ CDM model the Laplace approximations  $p_L(\Omega_m|\mathbf{d})$  and  $p_L(H_0|\mathbf{d})$  are shifted and narrower compared to the exact marginal distributions. The jumps in the profiling graph lead to discontinuities in these approximations.

In the data analysis of the Pantheon+ sample as well as in the examples from section 3 we always use flat priors to be able to compare marginal posterior distribution with the profiled posterior distribution on an equal footing. In a Bayesian analysis one could use either prior distributions which are motivated by subjective prior knowledge or objective priors, constructed from an extremalisation or based on invariance requirements. Then however the direct proportionality of the profiled posterior distribution with the profile likelihood is lost. Our aim in this work is the comparison of profiling and marginalisation and therefore we stick to the flat priors.

### 4.3 Summary of the one-dimensional distributions

In figure 10 we present a summary of the one dimensional marginal distributions for  $H_0$ ,  $\Omega_m$ ,  $\Omega_\Lambda$ ,  $\Omega_k$ , and  $w$  for all the models together with the corresponding profiled posterior distributions. The distribution of  $H_0$  shows only small variation between the models and between the marginal and profiled posterior distributions. This is not surprising since the value of  $H_0$  is determined mainly by the local SHOES sample [37]. The distributions of  $\Omega_m$  is

constrained strongest in the non-flat  $\Lambda$ CDM model. In the flat  $w$ CDM the distributions are consistent but slightly broader. This is also the case for the marginal posterior distribution in the non-flat  $w$ CDM model. But for this model the profiled posterior distribution of  $\Omega_m$  is strongly skewed towards smaller values and we mainly get an upper bound  $\Omega_m \lesssim 0.4$  from profiling. The marginal posterior distribution for  $\Omega_k = 1 - \Omega_m - \Omega_\Lambda$  is readily obtained from the Markov chains, but for the profiled posterior distribution we have to start new profiling runs. Both for  $\Omega_\Lambda$  and  $\Omega_k$  the distributions differ between the models. Specifically for the non-flat  $w$ CDM model the marginal posterior distributions of  $\Omega_\Lambda$  and  $\Omega_k$  are strongly skewed. Still they offer some localisation in parameter space. In this cases however the profiled posterior are essentially flat distributions offering only the bounds:  $0.2 \lesssim \Omega_\Lambda$ , and  $\Omega_m \lesssim 0.5$ , and  $-0.8 \lesssim \Omega_k \lesssim 0.7$ . A similar behaviour can be seen in the distribution of  $w$ . The marginal and especially the profiled posterior distribution only give the constraint  $w \lesssim -0.5$ . Showing the distributions of  $\Omega_k$  is redundant, but it illustrates nicely that the supernova magnitude redshift relation is only weakly constraining the curvature if one allows for  $w \neq -1$  (see e.g. [38]). Throughout we observe that the marginal posterior distributions give tighter constraints than the corresponding profiled posterior distributions.

The main aim of our article is to highlight the differences between profiling and marginalisation. Specifically the non-flat  $w$ CDM model shows several of the problems with the profiling procedure. From a physical perspective considering non-flat cosmological models with a uniform  $\Omega_k$  is only a first step. The curvature is a dynamical quantity. Using the scaling solution [39] from the backreaction approach Desgrange et al. [40] fit the supernova data without a dark energy component. Closely related, the timescape cosmologies provide a similar fit [41, 42]. Modelling the dark energy component with a constant equation of state parameter  $w$  can be viewed as the simplest case of an effective parameterisation [43, 44]. Further a parameterisations with orthonormal basis functions is possible [45]. Certainly a physical model for the dark energy component is needed. See Amendola et al. [46] for a review.

## 5 Conclusions

Instead of further summarising we will argue why one should use the marginal posterior distributions instead of the profiled posterior distribution or the profile likelihood to report results for parameter estimates.

Let us start with a formal argumentation based on the results from section 2. With the profiled posterior distribution we construct a Bayesian analogue of the profile likelihood. We show that the profiled posterior is a marginal posterior distribution of a Bayesian hierarchical model. The prior distribution of this hierarchical model forces the parameters of the model onto the profiling graph. We use flat prior distributions in all the calculations of the marginal posterior distribution presented here, since we want to compare with the profiled posterior distribution on an equal footing. Disregarding this connection we certainly may use different priors. The prior used for the hierarchical model from sect. 2.4 is one possibility. For this special prior the marginal posterior distribution equals the profiled posterior distribution. If we want to make statements about the parameters of the model by using the profiled posterior (respectively the profile likelihood) we also should explain why we choose this special prior. It is not clear to us what physical effect we can state, which is forcing the parameters onto the profiling graph.

Now let us consider the examples. In section 3 we identify two scenarios where the marginal differs from the profiled posterior distribution. First we construct a model with

a tuneable volume effect. With this nested model we are mimicking a situation observed for standard  $\Lambda$ CDM model embedded into the early dark energy model. We can tune the accessible parameter space volume in the two dimensional posterior distribution from a rather broad to a sharply peaked distribution. Similarly we can tune the resolution (or the precision) of the measurements in this example. The marginal posterior distribution stays invariant under this tuning, whereas the profiled posterior distribution is strongly depending on the available parameter space volume or the resolution. For a typically situation of parameter estimation the likelihood is given by the experimental or observational setup. We have no tuneable factor determining the available parameter space. The precision is determined by the measurement or observation procedure. Hence the marginal posterior distribution seems to be the appropriate choice for reporting results, if we want to be insensitive to variations of the resolution or the parameter space volume.

We also discuss a closely related model of Berger et al. [22]. Here the maximum of the posterior is on a ridge-like structure which itself is *not* surrounded by a region where a larger fraction of the posterior mass is accumulating. This maximum might not contribute appreciably to a marginal posterior distribution. However in this model the marginalisation, i.e. the volume integration, leads to a well defined marginal posterior distribution, whereas the maximisation results in an almost singular profiled posterior distribution.

From the examples and the Pantheon+ data analysis in section 4 we see that if the credible regions have a simple convex shapes then the profiled posterior and the marginal posterior distributions almost overlap. As soon as we observe non-convex credible regions, the profiled posterior and the marginal posterior distributions start to deviate. In some cases they even show a qualitatively different behaviour. We demonstrate discontinuous jumps in the profiling graph, which are not a numerical glitch, but an artefact of the method. An overly conservative approach might be to accept results only if the profiled and marginal posterior distributions agree. For the Rosenbrock function in section 3.4 and in the data analysis for the non-flat  $w$ CDM model in section 4.2.2 we have non-convex credible regions and we observe skewed marginal posterior distributions. Still these marginal posterior distributions offer some localisation in parameter space. However the corresponding profiled posterior distribution are essentially flat and offer only bounds. In addition, the ridge example in section 3.3 shows that the profiling can lead to an almost diverging profiled posterior distributions. Again we are led to the conclusion that the marginal posterior distribution is the stable and preferable way to report results for a parameter estimation.

## Acknowledgments

It is a pleasure to thank Steffen Hagstotz for comments and suggestions. This work would not have been possible without several libraries and tools. We would like to thank the creators of these tools, specifically we used Python with NumPy [47], SciPy [34], numdifftools [20], and Astropy<sup>3</sup> [30, 48, 49]. We used the affine invariant ensemble sampler emcee [32] to generate the Markov chains and ArviZ [50] to analyse them. For plots we were employing matplotlib [51] and `corner.py` [52].

---

<sup>3</sup><http://www.astropy.org>

## References

- [1] R. Trotta, *Bayes in the sky: Bayesian inference and model selection in cosmology*, *Contemporary Physics* **49** (2008) 71.
- [2] L. Herold, E.G.M. Ferreira and E. Komatsu, *New constraint on early dark energy from Planck and Boss data using the profile likelihood*, *Astrophys. J. Letters* **929** (2022) L16.
- [3] J. Hamann, *Evidence for extra radiation? Profile likelihood versus Bayesian posterior*, *JCAP* **2012** (2012) 021.
- [4] A.X. Gonzalez-Morales, R. Poltis, B.D. Sherwin and L. Verde, *Are priors responsible for cosmology favoring additional neutrino species?*, *arXiv e-prints* (2011) arXiv:1106.5052.
- [5] Planck Collaboration, P.A.R. Ade, N. Aghanim, M. Arnaud, M. Ashdown, J. Aumont et al., *Planck intermediate results. XVI. Profile likelihoods for cosmological parameters*, *Astron. Astrophys.* **566** (2014) A54 [1311.1657].
- [6] G.J. Feldman and R.D. Cousins, *Unified approach to the classical statistical analysis of small signals*, *Phys. Rev. D* **57** (1998) 3873.
- [7] J. Hamann, S. Hannestad, G.G. Raffelt and Y.Y.Y. Wong, *Observational bounds on the cosmic radiation density*, *JCAP* **2007** (2007) 021.
- [8] G. Efstathiou, E. Rosenberg and V. Poulin, *Improved planck constraints on axionlike early dark energy as a resolution of the Hubble tension*, *Phys. Rev. Lett.* **132** (2024) 221002.
- [9] A. Adil, A. Albrecht, R. Baunach, R. Holman, R.H. Ribeiro and B.J. Richard, *Entanglement masquerading in the CMB*, *JCAP* **2023** (2023) 024 [2211.11079].
- [10] P. Campeti and E. Komatsu, *New constraint on the tensor-to-scalar ratio from the planck and bicep/keck array data using the profile likelihood*, *Astrophys. J.* **941** (2022) 110.
- [11] A. Gómez-Valent, *Fast test to assess the impact of marginalization in monte carlo analyses and its application to cosmology*, *Phys. Rev. D* **106** (2022) 063506.
- [12] B. Hadzhiyska, K. Wolz, S. Azzoni, D. Alonso, C. García-García, J. Ruiz-Zapatero et al., *Cosmology with 6 parameters in the Stage-IV era: efficient marginalisation over nuisance parameters*, *The Open Journal of Astrophysics* **6** (2023) 23 [2301.11895].
- [13] M. Raveri, C. Doux and S. Pandey, *Understanding posterior projection effects with normalizing flows*, *arXiv e-prints* (2024) arXiv:2409.09101 [2409.09101].
- [14] E.O. Colgáin, S. Pourojaghi, M.M. Sheikh-Jabbari and D. Sherwin, *MCMC marginalisation bias and  $\Lambda$ CDM tensions*, *arXiv e-prints* (2023) arXiv:2307.16349 [2307.16349].
- [15] D. Scolnic, D. Brout, A. Carr, A.G. Riess, T.M. Davis, A. Dwomoh et al., *The Pantheon+ Analysis: The Full Data Set and Light-curve Release*, *Astrophys. J.* **938** (2022) 113.
- [16] L. Wassermann, *All of Statistics*, Springer Verlag, Berlin (2004), 10.1007/978-0-387-21736-9.
- [17] S.A. Murphy and A.W.V.D. Vaart, *On profile likelihood*, *Journal of the American Statistical Association* **95** (2000) 449.
- [18] R.E. Kass, L. Tierney and J.B. Kadane, *Laplace's method in Bayesian analysis*, *Contemporary Mathematics* **115** (1991) 89.
- [19] D.J.C. MacKay, *Bayesian Interpolation*, *Neural Computation* **4** (1992) 415.
- [20] P.A. Brodtkorb and J. D'Errico, *numdiff tools 0.9.41*, 2022.
- [21] L. Herold and E.G.M. Ferreira, *Resolving the Hubble tension with early dark energy*, *Phys. Rev. D* **108** (2023) 043513.
- [22] J.O. Berger, B. Liseo and R.L. Wolpert, *Integrated likelihood methods for eliminating nuisance parameters*, *Statistical Science* **14** (1999) 1.

- [23] J.A. Montoya, E. Díaz-Francés and D.A. Sprott, *On a criticism of the profile likelihood function*, *Statistical papers* **50** (2009) 195.
- [24] H. Rosenbrock, *An automatic method for finding the greatest or least value of a function*, *The computer journal* **3** (1960) 175.
- [25] J. Goodman and J. Weare, *Ensemble samplers with affine invariance*, *Communications in Applied Mathematics and Computer Science* **5**, No.1 (2010) 65.
- [26] Z. Wang, M. Broccardo and J. Song, *Hamiltonian monte carlo methods for subset simulation in reliability analysis*, *Structural Safety* **76** (2019) 51.
- [27] F. Pagani, M. Wiegand and S. Nadarajah, *An  $n$ -dimensional Rosenbrock distribution for markov chain monte carlo testing*, *Scandinavian Journal of Statistics* **49** (2022) 657.
- [28] S. Perlmutter, *Nobel lecture: Measuring the acceleration of the cosmic expansion using supernovae*, *Rev. Mod. Phys.* **84** (2012) 1127.
- [29] D. Brout, D. Scolnic, B. Popovic, A.G. Riess, A. Carr, J. Zuntz et al., *The Pantheon+ Analysis: Cosmological Constraints*, *Astrophys. J.* **938** (2022) 110.
- [30] Astropy Collaboration, A.M. Price-Whelan, P.L. Lim, N. Earl, N. Starkman, L. Bradley et al., *The Astropy Project: Sustaining and Growing a Community-oriented Open-source Project and the Latest Major Release (v5.0) of the Core Package*, *Astrophys. J.* **935** (2022) 167.
- [31] Planck Collaboration, N. Aghanim, Y. Akrami, M. Ashdown, J. Aumont, C. Baccigalupi et al., *Planck 2018 results. VI. Cosmological parameters*, *Astron. Astrophys.* **641** (2020) A6.
- [32] D. Foreman-Mackey, D.W. Hogg, D. Lang and J. Goodman, *emcee: The MCMC Hammer*, *PASP* **125** (2013) 306.
- [33] A. Vehtari, A. Gelman, D. Simpson, B. Carpenter and P.-C. Bürkner, *Rank-Normalization, Folding, and Localization: An Improved  $\hat{R}$  for Assessing Convergence of MCMC (with Discussion)*, *Bayesian Analysis* **16** (2021) 667 .
- [34] P. Virtanen, R. Gommers, T.E. Oliphant, M. Haberland, T. Reddy, D. Cournapeau et al., *SciPy 1.0: Fundamental Algorithms for Scientific Computing in Python*, *Nature Methods* **17** (2020) 261.
- [35] G. Boerner and J. Ehlers, *Was there a big bang?*, *Astron. Astrophys.* **204** (1988) 1.
- [36] J.M. Overduin and F.I. Cooperstock, *Evolution of the scale factor with a variable cosmological term*, *Phys. Rev. D* **58** (1998) 043506.
- [37] A.G. Riess, L.M. Macri, S.L. Hoffmann, D. Scolnic, S. Casertano, A.V. Filippenko et al., *A 2.4% determination of the local value of the Hubble constant*, *Astrophys. J.* **826** (2016) 56.
- [38] M. Kowalski, D. Rubin, G. Aldering, R.J. Agostinho, A. Amadon, R. Amanullah et al., *Improved Cosmological Constraints from New, Old, and Combined Supernova Data Sets*, *Astrophys. J.* **686** (2008) 749.
- [39] T. Buchert, J. Larena and J.-M. Alimi, *Correspondence between kinematical backreaction and scalar field cosmologies—the ‘morphon field’*, *Class. Quantum Grav.* **23** (2006) 6379.
- [40] C. Desgrange, A. Heinesen and T. Buchert, *Dynamical spatial curvature as a fit to type Ia supernovae*, *International Journal of Modern Physics D* **28** (2019) 1950143.
- [41] L.H. Dam, A. Heinesen and D.L. Wiltshire, *Apparent cosmic acceleration from type Ia supernovae*, *Mon. Not. Roy. Astron. Soc.* **472** (2017) 835.
- [42] Z.G. Lane, A. Seifert, R. Ridden-Harper, J. Wagner and D.L. Wiltshire, *Cosmological foundations revisited with Pantheon+*, *arXiv e-prints* (2023) arXiv:2311.01438 [2311.01438].
- [43] M. Chevallier and D. Polarski, *Accelerating universes with scaling dark matter*, *International Journal of Modern Physics D* **10** (2001) 213.

- [44] E.V. Linder, *Exploring the expansion history of the Universe*, *Phys. Rev. Lett.* **90** (2003) 091301.
- [45] J. Wagner and S. Meyer, *Generalized model-independent characterization of strong gravitational lenses V: reconstructing the lensing distance ratio by supernovae for a general Friedmann universe*, *Mon. Not. Roy. Astron. Soc.* **490** (2019) 1913.
- [46] L. Amendola, S. Appleby, A. Avgoustidis, D. Bacon, T. Baker, M. Baldi et al., *Cosmology and fundamental physics with the Euclid satellite*, *Living Reviews in Relativity* **21** (2018) 2 [1606.00180].
- [47] C.R. Harris, K.J. Millman, S.J. van der Walt, R. Gommers, P. Virtanen, D. Cournapeau et al., *Array programming with NumPy*, *Nature* **585** (2020) 357.
- [48] Astropy Collaboration, T.P. Robitaille, E.J. Tollerud, P. Greenfield, M. Droettboom, E. Bray et al., *Astropy: A community Python package for astronomy*, *Astron. Astrophys.* **204** (1988) 1.
- [49] Astropy Collaboration, A.M. Price-Whelan, B.M. Sipőcz, H.M. Günther, P.L. Lim, S.M. Crawford et al., *The Astropy Project: Building an Open-science Project and Status of the v2.0 Core Package*, *Astronom. J.* **156** (2018) 123.
- [50] R. Kumar, C. Carroll, A. Hartikainen and O. Martin, *Arviz a unified library for exploratory analysis of bayesian models in python*, *Journal of Open Source Software* **4** (2019) 1143.
- [51] J.D. Hunter, *Matplotlib: A 2d graphics environment*, *Computing In Science & Engineering* **9** (2007) 90.
- [52] D. Foreman-Mackey, *corner.py: Scatterplot matrices in python*, *The Journal of Open Source Software* **1** (2016) 24.